Int. J. Electrochem. Sci., 8 **(2013)** 1394 - 1408

International Journal of
ELECTROCHEMICAL
SCIENCE
www.electrochemsci.org

Sol-gel Derived Biphasic Calcium Phosphate Ceramics on Nitinol for Medical Applications

Jozefina Katić[1], *Mirjana Metikoš-Huković*[1,*], *Ranko Babić*[1], *Marijan Marciuš*[2]

[1] Department of Electrochemistry, Faculty of Chemical Engineering and Technology, University of Zagreb, P.O. Box 177, 10000 Zagreb, Croatia
[2] Laboratory for Synthesis of New Materials, Division of Materials Chemistry, Institute Ruđer Bošković, Bijenička cesta 54, 10000 Zagreb, Croatia
[*]E-mail: mmetik@fkit.hr

Received: 19 November 2012 / *Accepted:* 7 December 2012 / *Published:* 1 January 2013

Nitinol is an attractive material for various types of medical implants due to its superior mechanical and unique properties (shape memory effect, superelasticity, high damping capacity etc). The Nitinol surface was modified with biocompatible coatings of calcium phosphate prepared by the sol-gel dip-coating method. The surface morphology, structure, and chemical composition of coatings were investigated by field emission scanning electron microscopy (FE – SEM)/energy dispersive X-ray spectroscopy (EDS), and Fourier transform infrared spectroscopy (FTIR). The barrier properties were investigated *in vitro* in simulated physiological solution using electrochemical impedance spectroscopy (EIS). It has been shown that the cycling dip-coating-calcining procedure produces homogeneous films with excellent barrier properties.

Keywords: materials science, Nitinol, biphasic calcium phosphate, sol-gel method, biocompatibility, spectroscopic methods

1. INTRODUCTION

Titanium and its alloys have been extensively used as dental and orthopedic implant materials due to their good biocompatibility, superior mechanical strength, durability, and corrosion resistance [1,2]. Besides the other titanium alloys (e.g. titanium-aluminum-vanadium, and titanium-aluminum-niobium), Nitinol (NiTi) has been widely used in the field of orthopedic surgery [3,4] owing to its unique properties, such as shape memory effect, superelasticity, and high damping capacity [5]. Although Nitinol possess high corrosion resistance in physiological solutions caused by the spontaneously formed passive film of TiO_2 [5,6], the major concern regarding its biocompatibility is release of allergenic and toxic Ni^{2+} ions [7] due to *in vivo* corrosion. Thus, to improve its corrosion resistance and prevent nickel dissolution, Nitinol has been modified using different surface treatments including coatings [8-10].

Nitinol and Ti-based alloys are classified as bioinert materials as they do not induce bone formation on their surface [11]. An achieved integrity and structural continuity of implant material with surrounding bone are of extreme importance for *in vivo* behavior and a longer life-time of implants [12]. Hence, the formation of calcium phosphates (CaPs) coating serves as a good barrier to Nitinol degradation and combines good mechanical properties of the metallic substrate with a good bio-behavior of coatings [1,13-16]. It is necessary to stress that the bioactive concept, developed for biphasic calcium phosphate ceramics, is based on an optimum balance of the more stable phase of hydroxyapatite (HAp) and more soluble tricalcium phosphate (TCP), depending on the application aspect. Thus, the presence of TCP in the bioceramic material is not necessarily detrimental as was considered earlier, since its rate of dissolution is greater than that of HAp in physiological environments [17]. TCP gradually dissolves in the body and a biological calcium phosphate layer precipitates and leads to a more effective bone regeneration ability [18]. Hence, low content of TCP in bioceramic material is helpful for the enhanced osseointegration [19].

Different methods have been used for the formation of CaP coatings on titanium/titanium alloys: sol-gel, electrocrystallization, electrophoretic deposition, electrochemical deposition, laser-pulse deposition and plasma or thermal spraying [13,20]. The sol-gel method followed by calcination has gained more attention for producing adherent, dense and crystalline coating [21-23].

In the present paper Nitinol was protected with CaP coatings using a sol-gel method. The microstructure of CaP coatings was characterized by field emission scanning electron microscopy (SEM). The chemical composition was examined using energy dispersive X-ray spectroscopy (EDS), Fourier transform infrared spectroscopy (FTIR), and X-ray diffraction analysis (XRD). The barrier properties of coatings were tested in a physiological Hanks' solution using electrochemical impedance spectroscopy (EIS).

2. EXPERIMENTAL

2.1. Sol-gel synthesis/preparation

10 g of calcium 2-ethylhexanoate ($Ca(EHA)_2$; wt98%, Aldrich) was dissolved in 28.6 mL of ethylhexanoic acid (EHA; wt99%, Aldrich). To produce the sol of calcium phosphate with Ca/P molar ratio of 1.67, the above solution was mixed with 4.76 mL of 2-ethylhexyl-phosphate (EHP; 95 wt%, Merck, mixture of 45% mono- and 55% di-ester of phosphoric acid). After adding ethanol to reduce the overall calcium phosphate concentration to 5 wt%, the sol was stirred at 21±2 °C for 4 h before being used for coating. The sol was dried at 130 °C for 4 h and the resulting yellow sticky gel was calcined at 450 and 600 °C for further characterization.

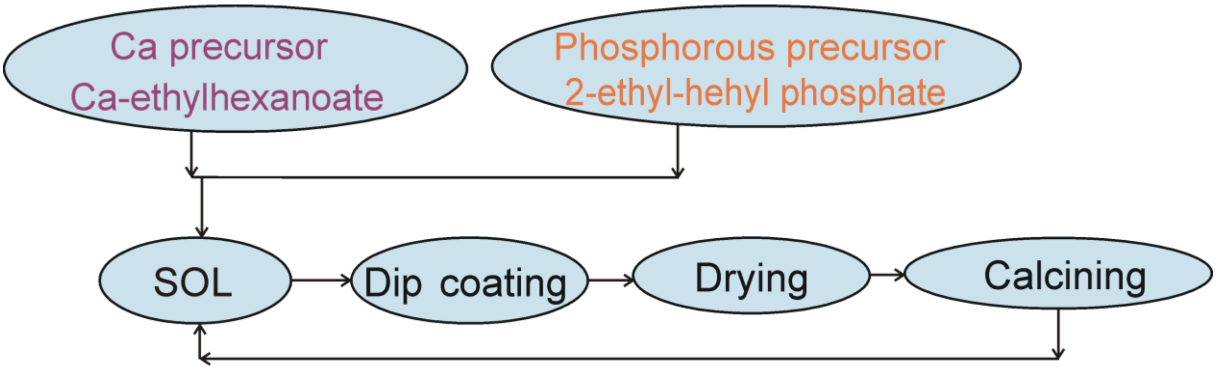

Figure 1. The flow chart of the sol synthesis and coating formation.

2.1.1. Methods for gel characterization

Simultaneous differential thermal analysis (used in DSC mode) and thermogravimetry (DSC-TGA) were carried out using Netzsch STA 409 to determine the thermal behavior of prepared gels with the constant air flow of 30 cm^3 min^{-1} and at the heating rate of 10 K min^{-1}. Phase analysis was accomplished by XRD. The XRD patterns were recorded at 20±2 °C using APD 2000 X-ray powder diffractometer (CuKα radiation, 2θ step of 0.02° / 10 s, graphite monochromator, NaI-Tl detector) manufactured by *ItalStructures*, Riva Del Garda, Italy.

2.2. Dip-coating procedure

The Nitinol foil (Alfa Aesar with wt% content: Ni 55.82, C ≤ 0.05, O ≤ 0.05, other metal impurities ≤ 0.20, and Ti balance) was cut into 0.38 mm-thick disks of 13 mm in diameter. Circular-shaped Nitinol samples were successively abraded with SiC papers of #240 to #1200 grit size followed by ultrasonic cleaning with acetone and redistilled water. The freshly prepared Nitinol samples were kept at 90 °C for 30 min in a regular air-convection oven. The coating was formed by dipping the samples into the CaP sol at 21±2 °C, pulling them out at a speed of approximately 6 cm min^{-1}, drying in air at 130 °C for 4 h, and calcining in a preheated furnace at 450 and 600 °C for 10 minutes. The multilayered coatings on Nitinol were prepared by cycling the above procedure.

2.2.1. Methods for coatings characterization

Field emission scanning electron microscopy/energy dispersive X-ray spectroscopy – The microstructure and morphology of the coatings on the Nitinol substrates were determined by SEM using *Jeol Ltd.* FE SEM, model JSM-7000F. An elemental analysis was performed by EDS using *Oxford Instruments Ltd*. EDS/INCA 350 in addition to SEM.

Fourier transform infrared spectroscopy - FTIR was used to determine the functional groups in CaP coatings. The spectra were recorded on Perkin Elmer Spectrum One FTIR spectrometer in the range of 4000 to 450 cm^{-1} with the scan resolution of 4 cm^{-1}.

Electrochemical impedance spectroscopy – The corrosion behavior of coated Nitinol was examined by EIS, which were performed in a standard three-electrode cell (PAR, Corrosion Cell System, Model K47) at 37°C in the Hanks' solution. A Solartron potentiostat/galvanostat (Model 1287) with FRA 1260 was used in these measurements. A reference electrode, to which all potentials in the paper are referred, was an Ag | AgCl, 3.0 mol dm^{-3} KCl (E = 0.210 V vs. SHE). Impedance measurements were performed at the open circuit potential (E_{OCP}) after one hour of stabilization of the working electrodes (uncoated and coated) in the Hanks' solution, with an *ac* voltage amplitude of ±5 mV and in the frequency range from 10^5 to 10^{-3} Hz. Impedance data were fitted by a suitable electrical equivalent circuit (EEC) model, employing the complex non-linear least squares (CNLS) fit analysis [24] offered by the Solartron *ZView*® software. The fitting quality was evaluated by the chi-squared and relative error values, which were in the order of 10^{-3}-10^{-4} and below 5 %, respectively, indicating that the agreement between the proposed EEC model and the experimental data was good.

3. RESULTS

3.1. Characterization of the CaP gel

The CaP gel, produced by drying the sol at 130 °C for 4 h, was subjected to DTA and TGA analyses. The scans obtained are presented in Fig. 2a. Several exothermic peaks can be observed in the temperature range from 50-1500 °C. The first one at 78 °C is ascribed to the adsorbed water and ethanol removal and is accompanied by small mass loss of 3 % in the corresponding TGA scan. The strong exothermic peak at 270 °C, weak exothermic peaks around 320 °C and around 400 °C followed by a large mass loss of 70 % (Fig. 2a) are attributed to evaporation of volatile components (EHA and EHP) [25] and burn-off of organic material [26]. The strong exothermic peaks at about 510 and 670 °C are attributed to the combustion of organic material and peaks at 400 and 520 °C are assigned to the phosphate crystallization [17,19,27]; these processes occur simultaneously. The strong endothermic peak at 700 °C is probably related to removal of residuals of organic compounds [28]. The TGA scan showed a small mass loss of 5 % at temperatures above 550 °C; an almost constant curve was noticed indicating thermal stability of dried sol.

To define the thermal behavior in detail, the powder sample was additionally calcined at 450 °C for 10 minutes to burn off the majority of organic material. The subsequent DTA/TGA (Fig. 2b) and XRD analyses of calcined gel were performed (Fig. 3). The DTA analysis (Fig. 2b) of calcined gel shows an exothermic peak at 78 °C followed by a 3% mass loss related to removal of adsorbed water and solvent as for non-calcined sample. The peaks observed at 420 and 550 °C and a broad peak at 700 °C lie on an exothermic rise. These peaks point to the phosphate crystallization and removal of residues of organic precursors, respectively [27,29,30]. The release of heat on crystallization is small, suggesting that a small atomic rearrangement of calcium and phosphate species is required for crystallization. The thermal behavior at temperatures higher than 800 °C is identical to that of the non-calcined gel. The corresponding TGA trace (Fig. 2b) showed a total mass loss of 15 % including the evaporation of absorbed water, the decomposition of organic compounds, and the phosphate crystallization.

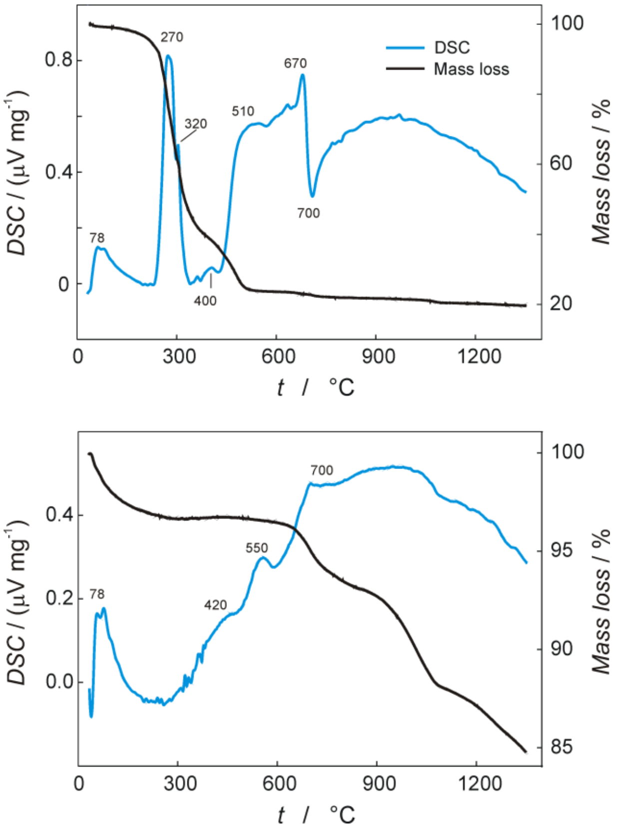

Figure 2. Results of DTA/TGA analysis of gel dried at 130 °C (a) and calcined at 450 °C (b).

Figure 3 presents the XRD pattern for the CaP powder calcined at 600 °C and 450 °C. The identification of phases was performed by comparing the experimental XRD patterns to standards compiled by the Joint Committee on Powder Diffraction Standards [31] using the cards no. 09-0432 for HAp, 85-1108 for calcite, and 29-0359 for tricalcium phosphate.

The XRD data indicate that the calcined powder is composed of HAp, tricalcium phosphate and calcite (Fig. 3). The HAp phase was identified from the XRD pattern based on the position and intensity of the diffraction peaks in the range 31.8-32.5° of 2θ values, which is characteristic for the apatite phase. These results are corroborated with the DTA results (Fig. 2); the exothermic peaks around 400 °C are associated with crystallization of hydroxyapatite. During the gel calcination, the organic matter is burned and produced CO_2 (Fig. 2) may become incorporated into the crystal structure in the form of calcium carbonate [23]. The increase in the calcining temperature favors the formation of the HAp phase with a small amount of tricalcium phosphate. The latter has ability to form biphase calcium phosphate (both HAp and TCP), which has been recently recognized as an offering material in clinical application [32] due to its controllable degradation rate and more effective bone regeneration ability [33].

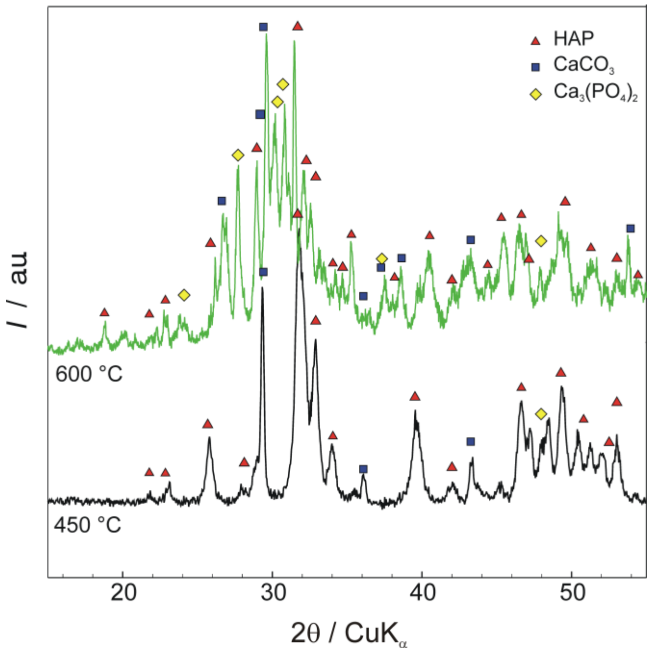

Figure 3. The XRD pattern for the gel calcined at 450 and 600 °C.

3.2. Characterization of CaP coatings on Nitinol

3.2.1. Field emission scanning electron microscopy

The microstructure and morphological characteristics of CaP coatings were characterized by SEM. The SEM images, presented in Fig. 4a,b, show a heterogeneous cracked morphology of a single-layer coatings consisting of flat/smooth areas and aggregated spherical and semi-spherical particles formed on flat/smooth areas. The SEM images reveal a “dried mud” type cracking configuration that is indicative of high shrinkage [34]. The formation of cracks occurs due to densification and thermal stresses originated from the mismatch between thermal expansions coefficients of metallic substrate covered with oxide layer (TiO_2) thermally formed and CaP coating [11,35]. The increase in calcination temperature makes the structure of coating more compact and agglomerates became more condense, but does not eliminate the presence of pores/cracks; (not presented here).

Figure 4(c-f) presents SEM images of multi-layer coatings. From the sample top view, a relatively homogenous distribution of a deposit on a large length scale could be observed at all samples. It is clearly evident that multiple-coating process produces very compact CaP coatings without cracks/pores. A multi-layered CaP coating strategy was successful in formation of indented bone-like structure (Fig. 4) [36].

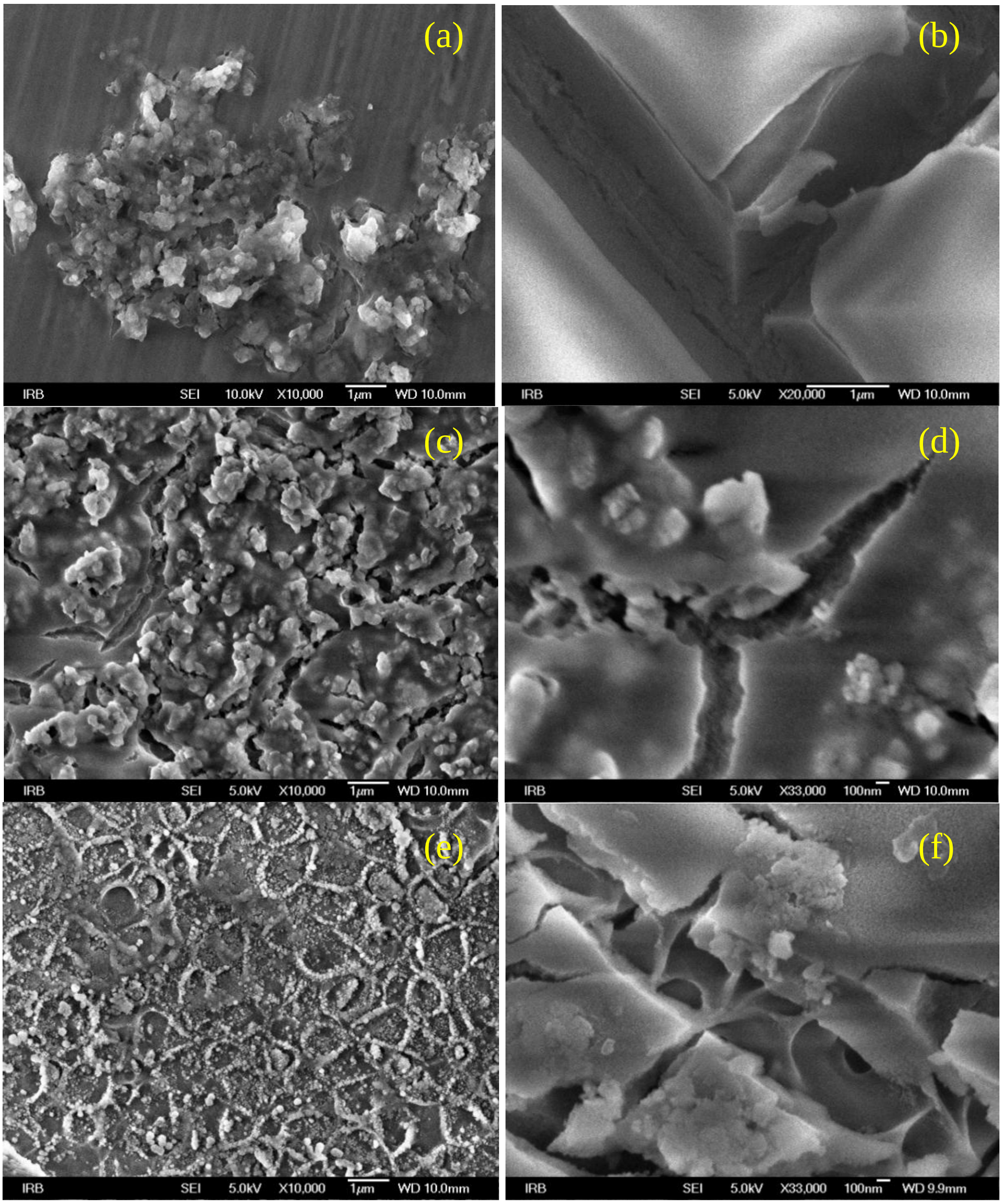

Figure 4. SEM images of coated Nitinol substrates by 1 (a,b), 5 (c,d) and 10 CaP layers (e,f) calcined at 450 °C.

Using SEM, the map for each element of interest was obtained on the single-layer coatings. Various color intensities were used to visualize the concentration of each specific element across the area being inspected. Fig. 5 shows a SEM image and corresponding mapping images of Ca, O, P, Ti and Ni of the Nitinol substrate coated by a single CaP layer. The elemental distribution shows only the presence of Ca, P and O at the island like/flat surfaces. At the pore areas Ti-rich regions are observed due to the presence of TiO_2.

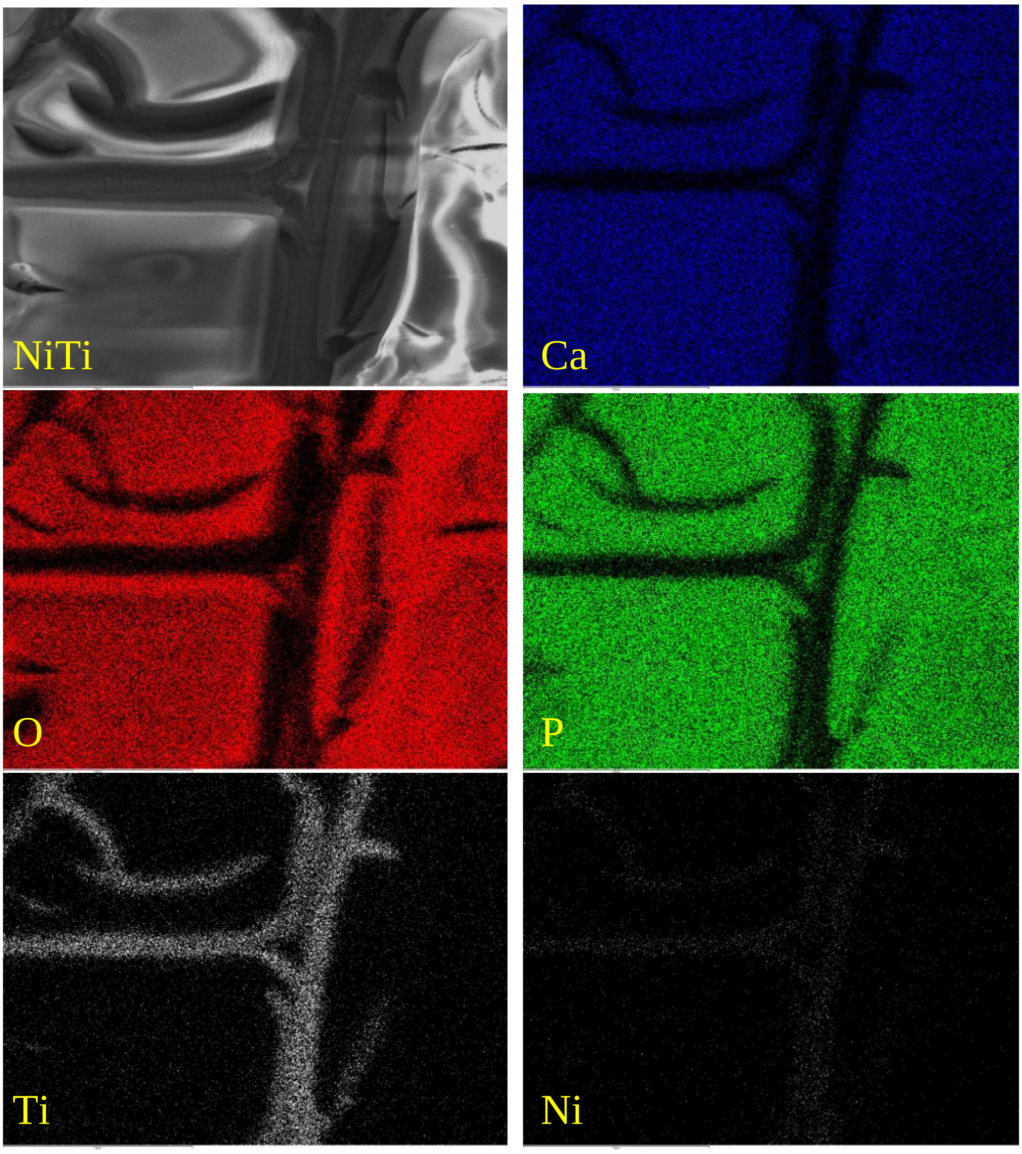

Figure 5. The SEM image (a) and elemental mapping images of CaP coated Nitinol substrates: Ca (b), O (c), P (d), Ti (e), Ni (f).

3.2.2. Energy dispersive X-ray spectroscopy

To identify the chemical nature of CaP coatings in detail, the EDS analysis was performed at the places of interest: in the pores/cracks (Fig. 6a), in the particle agglomerate areas/flat surfaces on the single- (Fig. 6b) and multilayer (Fig. 6c) CaP coatings. The EDS results support the results presented in Figs. 4 and 5.

The single-layered coatings show a Ca/P molar ratio of approximately 1.41 (Fig. 6b), indicating a composition close to physiological HAp (Ca/P molar ratio is 1.35-1.46) [35]. The EDS analysis performed on multi-layered CaP coatings (Fig. 6c) does not show any trace of Ti or Ni metal signals on the overall surface confirming the complete coverage of the substrate. The Ca/P molar ratio of these coating is 1.57, which closely resembles a human bone apatite [37].

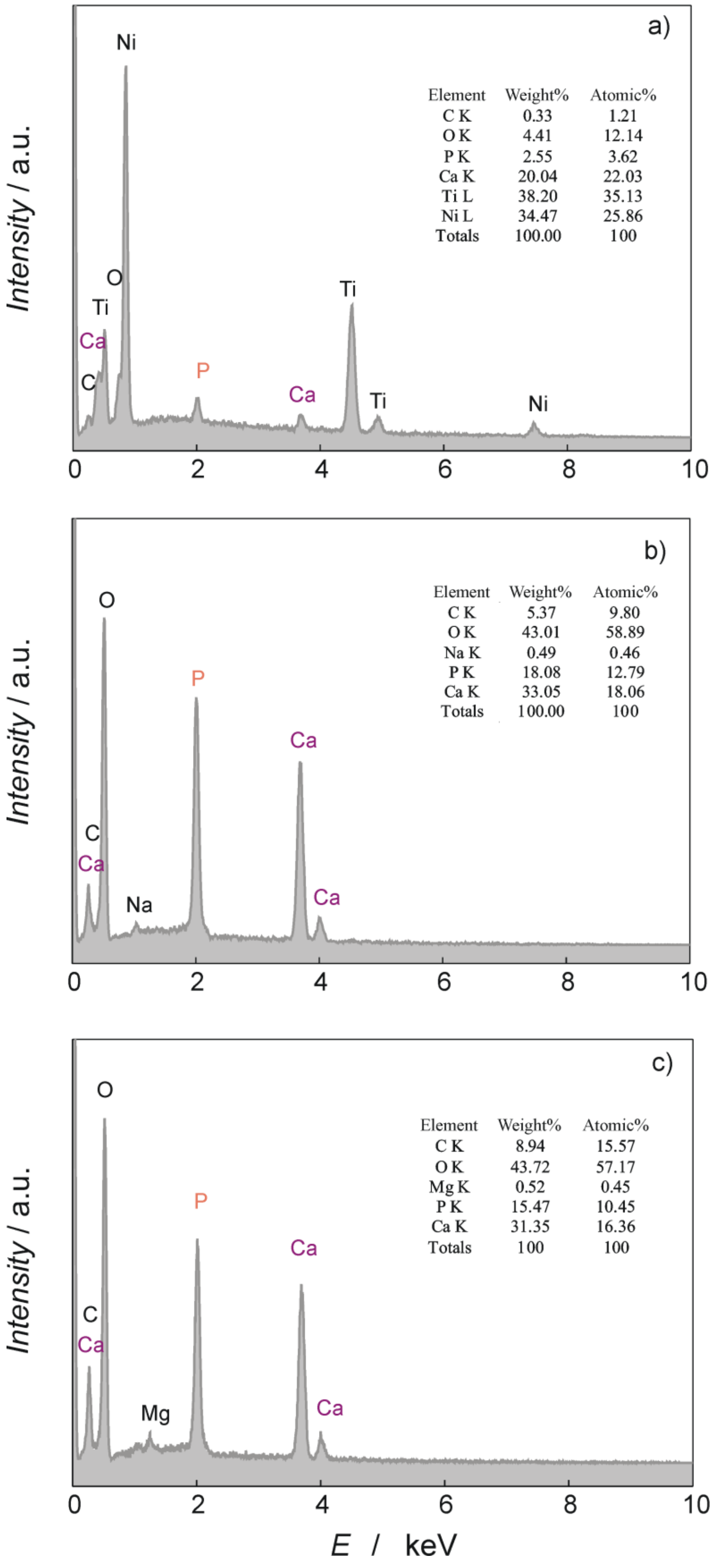

a)

Element	Weight%	Atomic%
C K	0.33	1.21
O K	4.41	12.14
P K	2.55	3.62
Ca K	20.04	22.03
Ti L	38.20	35.13
Ni L	34.47	25.86
Totals	100.00	100

b)

Element	Weight%	Atomic%
C K	5.37	9.80
O K	43.01	58.89
Na K	0.49	0.46
P K	18.08	12.79
Ca K	33.05	18.06
Totals	100.00	100

c)

Element	Weight%	Atomic%
C K	8.94	15.57
O K	43.72	57.17
Mg K	0.52	0.45
P K	15.47	10.45
Ca K	31.35	16.36
Totals	100	100

Figure 6. The EDS analysis of CaP coatings: in the pores/cracks (a), in the particle agglomerates area/on the flat surfaces on Nitinol substrate coated by 1 (b) and 10 layers (c).

3.2.3. Fourier transform infrared spectroscopy

The FTIR spectra of uncoated and CaP coated Nitinol samples are presented in Fig. 7. They clearly illustrate typical bands of apatite structure: characteristic ν_4 PO_4^{3-} bands at 560-600 cm^{-1} (O-P-O bending vibrations), ν_1 PO_4^{3-} band at 903 cm^{-1} (P-O symmetric stretching vibrations) and a strong ν_3 PO_4^{3-}absorption band in the range 1100-1000 cm^{-1} (P-O asymmetric stretching vibrations) [15,21,38-40].

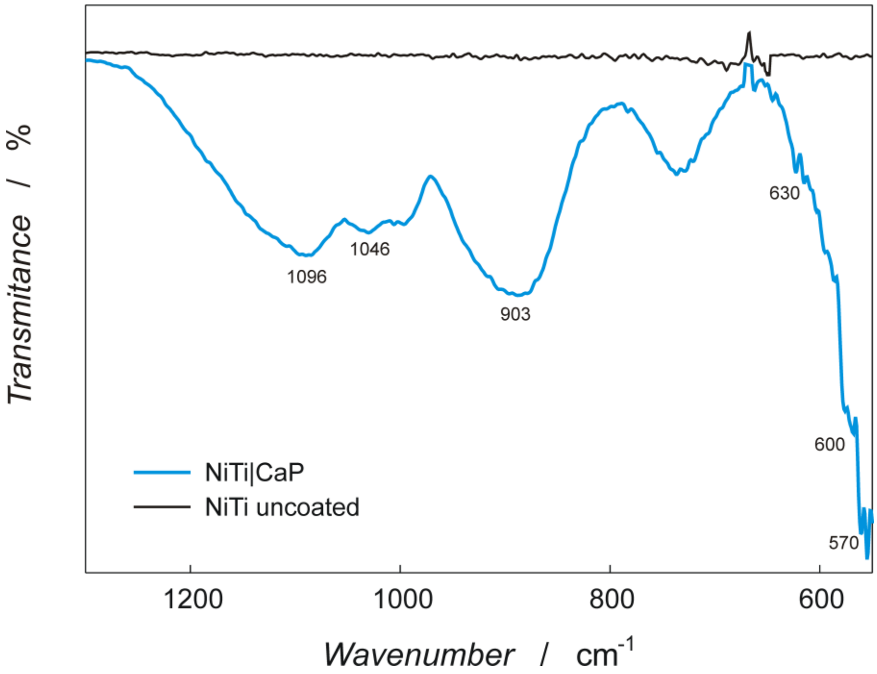

Figure 7. FTIR spectra of uncoated and CaP coated Nitinol samples calcined at 600 °C.

The P-O deformation (570 and 600 cm^{-1}) and vibration bands (1046 and 1090 cm^{-1}) became more separated and stronger with the increase in calcination temperature. Two bands at about 3570 cm^{-1} (not presented here) and at 630 cm^{-1} are derived from stretching and vibrational modes of OH groups in hydroxyapatite [15,29]. The bands observed in the region 1750-1400 cm^{-1} (not presented here) can be ascribed to C-O and C=O vibration of organic residues or to C=O vibration of carbonate groups in calcite [38,41]. These results as well as the EDS ones show that the CaP coatings obtained by a sol-gel procedure contain tricalcium phosphate, hydroxyapatite and a small amount of calcite. The presence of tricalcium phosphate in the coating mimics the bone composition and gives an added advantage because it leads to an enhanced osseointegration [11].

3.3. Barrier properties of CaP coatings on Nitinol

Barrier properties of CaP coatings on Nitinol were examined in the Hanks' solution by using EIS as a nondestructive method. In order to quantify the contribution of the CaP coating to barrier properties of the NiTi|CaP|physiological solution interface, EIS spectra were recorded on Nitinol with a native oxide layer and CaP coated Nitinol (dried and thermally treated). Since the oxide film grows and thicknesses during the thermal treatment of CaP coatings, the impedance spectra were recorded with the system Nitinol|therm. oxide|electrolyte to resolve the influence of the oxide layer on the barrier properties of the CaP coating.

As an example, the impedance spectra recorded on Nitinol electrodes are presented in Fig. 8 as Bode plots. All spectra were fitted to the proposed electrical equivalent circuit (EEC) with one time constant; an electrolyte resistance (R_{el})□ in a series with the parallel combination of the film/coating resistance (R) and the interfacial capacitance (C). The corresponding EEC parameters are listed in Table 1.

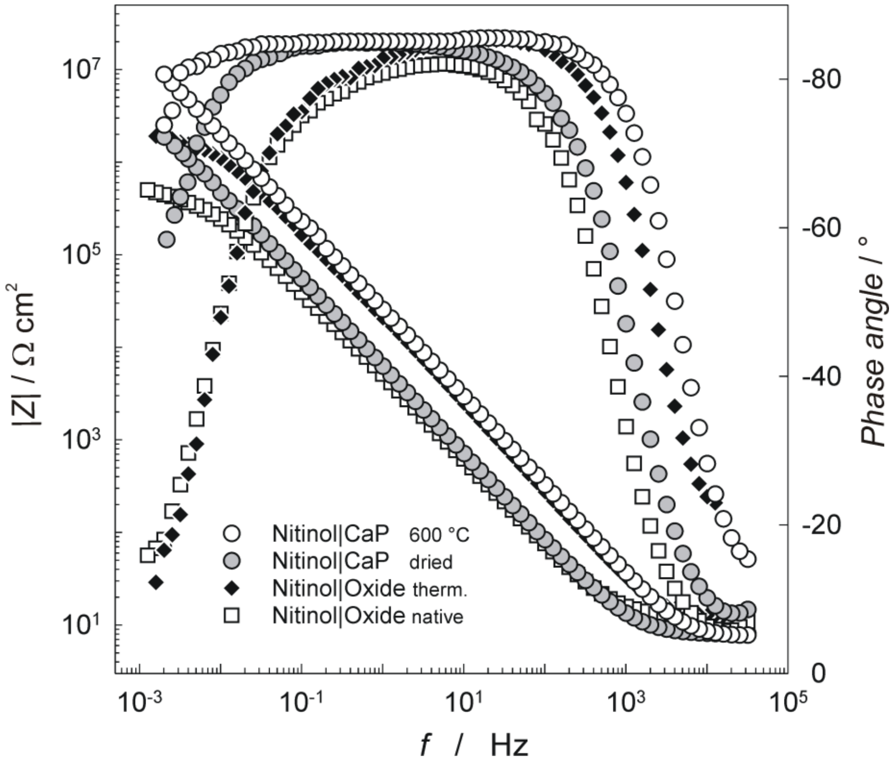

Figure 8. The Bode plot of impedance spectra recorded on Nitinol specimens in Hanks' solution (37 °C) at E_{OCP}.

Table 1. Impedance parameters of Nitinol samples obtained in Hanks' solution.

Samples	*R* / MΩ cm^2	*C* / µF cm^{-2}
NiTi | CaP, 600 °C	44.5	3.35
NiTi | CaP, 450 °C	34.4	6.70
NiTi | CaP, dried 130 °C	4.12	13.7
NiTi | Therm. ox. 600 °C	1.81	3.57
NiTi | Therm. ox. 450 °C	3.01	4.53
NiTi | Native oxide	0.46	14.8

$R_{el} = 21 \pm 5\ \Omega\ cm^2$

The data obtained show that the film resistance increases significantly during calcination and achieves values two orders of magnitude higher than that of Nitinol with a native oxide layer. A decrease in capacitance for samples thermally treated addresses to structural changes in the coating.

The EIS spectra of NiTi electrodes covered with multilayered CaP coatings (5 and 10 layers) and calcined at 600 °C are presented in Fig. 9 as complex plane plots: Z_{imag} versus Z_{real} and C_{imag} versus C_{real}. The data for a latter dependence were calculated using Eq (1) [42]:

$$C(\omega) = 1/(j\omega Z) = C_{\mathrm{real}} + jC_{\mathrm{imag}} = \frac{C}{1+(\omega R_{\mathrm{el}}C)^2} - j\frac{R_{\mathrm{el}}\omega(C)^2}{1+(\omega R_{\mathrm{el}}C)^2} \qquad (1)$$

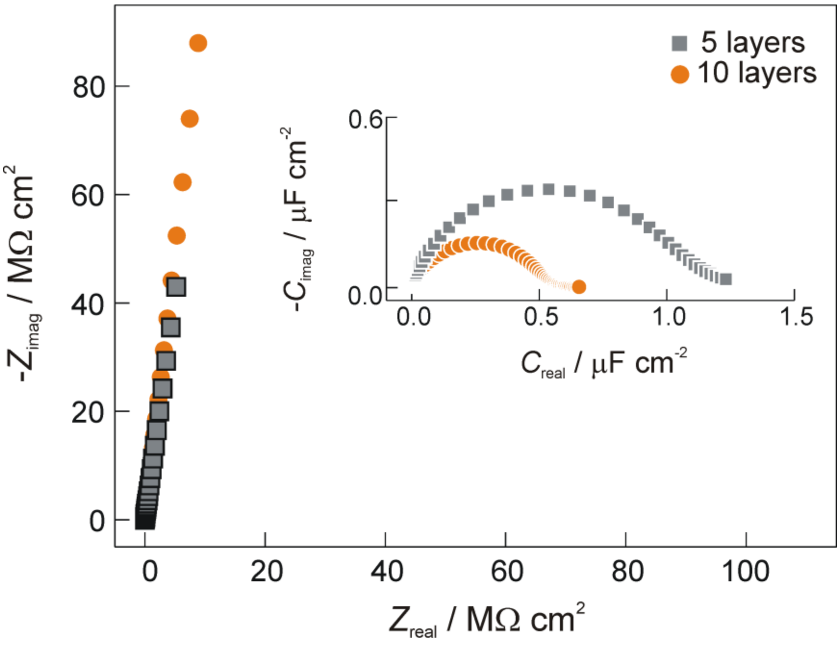

Figure 9. The complex plane plot of impedance data for NiTi|multilayered CaP samples calcined at 600 °C recorded in Hanks' solution (37°C) at E_{OCP}. The insert: C_{imag} versus C_{real}.

The EIS response presented in the Nyquist plot for all multilayerd CaP oatings are almost parallel to the axis of the impedance imaginary part, (Z_{imag}). This behavior as well as capacitance loops in the Cole-Cole diagram is characteristic for the blocking electrode|solution interface. For these systems, the charge transfer resistance $R \to \infty$, and the corrosion current $\to 0$, what means that the corrosion of metal substrate, i.e., the dissolution of nickel can be ignored as long as the coating posses these properties. The corresponding EEC for the blocking electrode consists of a CPE in series with an electrolyte resistance. Its impedance is defined [43]:

$$Z(f) = R_{\mathrm{el}} + 1/[j2\pi f C] \qquad (2)$$

where the parameter C is the interfacial capacitance. The parameter values are listed in Table 2.

Table 2. Impedance parameters of Nitinol samples obtained in Hanks' solution.

NiTi|CaP	450 °C 5 layers	600 °C 5 layers	450 °C 10 layers	600 °C 10 layers
C / μF cm^{-2}	1.26	0.90	0.40	0.44

$R_{el} = 21 \pm 5\ \Omega\ cm^2$

4. CONCLUSIONS

The XRD and FTIR data have shown that the calcined CaP powder as well as the CaP coatings on Nitinol is composed of HAp, TCP with a small addition of calcite. Thus, the CaP coating on Nitinol, obtained by a sol-gel method, represents biphasic calcium phosphate bioceramics.

The crystallization process of CaP was studied using DTA/TGA analyses. It takes place at temperatures above 400 ^{o}C.

The single-layer coatings show cracked morphology due to different thermal expansion coefficients of the Nitinol substrate and the CaP coating. The strategy of multi-layer coatings, produced on the oxide layer, was shown to be successful in formation of homogeneous and dense coatings. We hypothesize that this is a result of the coating densification during the calcination and the influence of difference in thermal coefficients of Nitinol and coating decreases.

The barrier properties of the system:

Nitinol | oxide film | CaP coating | simulated physiological solution

were investigated in situ using impedance spectroscopy. The multilayer coating acts as an effective barrier between Nitinol and the aggressive environment, which prevents transport of allergenic nickel ions into bio environments.

The sol-gel formed biphasic calcium phosphate coatings, having excellent barrier and morphological properties, belong to a set of bioceramic materials, which offer the opportunity to create a grafting material with high bioactivity, bioresorbility and biocompatibility. TCP is biodegradable in vivo and its low content in CaP coatings could be helpful for the enhanced osseointegration, i.e., a rapid bonding of implants to the natural bone.

ACKNOWLEDGEMENTS
The financial support provided by the Ministry of Science, Education and Sports of the Republic of Croatia is greatly appreciated.

List of symbols

C	capacitance (F cm^{-2})
C_{imag}	imaginaty part of the capacitance (F cm^{-2})
C_{real}	real part of the capacitance (F cm^{-2})

CPE	constant phase element
E	energy (eV)
E	potential (V)
E_{OCP}	open circuit potential (V)
f	frequency (Hz)
I	intensity (a.u.)
$\mathrm{j}\omega$	complex variable for sinusoidal perturbations with $\omega = 2f\pi$
R	resistance (Ω cm^2)
R_{el}	ohmic resistance □(Ω cm^2)
Z	electrode impedance (Ω cm^2)
$\|Z\|$	impedance modulus (Ω cm^2)
Z_{imag}	imaginary part of the impedance (Ω cm^2)
Z_{real}	real part of the impedance (Ω cm^2)

Greeks letters

θ	diffraction angle (°)
v	wavenumber (cm^{-1})
ω	angular frequency (Hz)

References

1. B. D. Ratner, A. S. Hoffman, F. J. Schoen and J. E. Lemons (Eds.), *Biomaterials Science, An Introduction to Materials in Medicine*, Academic Press, San Diego (1996)
2. D.F. Williams (Ed.), *Biocompatibility of clinical implant materials,* CRC Press, Boca Raton (1981)
3. J. Musialek, P. Filip and J. Nieslanik, *Arch. Orthop. Trauma Surg.*, 117 (1998) 341
4. W. Xu, T. G. Frank, G. Stockham and A. Cuschieri, *Ann. Biomed. Eng.*, 27 (1999) 663
5. S.A. Shabalovskaya, *Bio-Med. Mater. Eng.*, 12 (2002) 69
6. N.Figuerira, T.M. Silva, M.J. Carmezin and J.C.S. Fernandes, *Electrochim. Acta*, 54 (2009) 921
7. D. Granchi, G. Ciapetti, L. Savarino, S. Stea, F. Filippini, A. Sudanese, R. Rotini and A. Giunti, *Biomaterials*, 21 (2000) 2059
8. S.A. Shabalovskaya, J. Anderegg and J. van Humbeeck, *Acta Biomater.*, 4 (2008) 447
9. X. Liu, P.K. Chu and C. Ding, *Mater. Sci. Eng.*, R47 (2004) 49
10. Ž. Petrović, J. Katić, M. Metikoš-Huković, H. Dadafarin and S. Omanovic, *J. Electrochem. Soc.*, 158 (2011) 159
11. L. Mohan, D. Durgalakshmi, M. Geetha, T.S.N. Sankara Narayanan and R. Asokamani, *Ceram. Inter.*, 38 (2012) 3435
12. P. Ducheyne and Q. Qiu, *Biomaterials*, 20 (1999) 2287
13. S.R. Paital and N. B. Dahotre, *Mater. Sci. Eng.*, R66 (2009) 1
14. L.L. Hench, *J. Am. Ceram. Soc.*, 81 (1998) 1705
15. A. Stoch, W. Jastrzebski, E. Dlugon, W. Lejda, B. Trybalska, G.J. Stoch and A. Adamczyk, *J. Molecul. Struct.*, 744-747 (2005) 633
16. J.X. Zhang, R.F. Guan and X.P. Zhang, *J. Alloys Compounds*, 509 (2011) 4643
17. U. Vijayalakshmi Natarajan and S. Rajeswari, *J. Cryst. Growth*, 310 (2008) 4601
18. J.C. Le Huec, D. Clement, B. Brouillaud, N. Barthe, B. Dupuy, B. Foliguet and B. Basse-Cathalinat, *Biomaterials*, 19 (1998) 733

19. S. R. Ramanan and R. Venkatesh, *Mater. Letts.*, 58 (2004) 3320
20. J. Weng, Q. Liu, J.G.C. Wolke, X. Zhang and K. de Groot, *Biomaterials*, 18 (1997) 1027
21. D.-M. Liu, Q. Yang and T. Troczynski, *Biomaterials*, 23 (2002) 691
22. W. Weng and J.L. Baptista, *J. Amer. Ceram. Soc.*, 82 (1999) 27
23. K.A.Gross, C.S. Chai, G.S.K. Kannangara, B. Ben-Nissan and L. Hanley, *J. Mater. Sci. Mater. Med.*, 9 (1998) 839
24. A. Boukamp, *Solid State Ionics*, 20 (1986) 31
25. http://www.sigmaaldrich.com/catalog/product/aldrich
26. E. Tkalcec, M. Sauer, R. Nonninger and H. Schmidt, *J. Mater. Sci.*, 36 (2001) 5253
27. D.-M. Liu, Q. Yang, T. Troczynski and W. J. Tseng, *Biomaterials*, 23 (2002) 1679
28. C.E. Wen, W. Xu, W.Y. Hu and P.D. Hodgson, *Acta Biomater.*, 3 (2007) 403
29. K.A. Gross, V. Gross and C.C. Berndt, *J. Amer. Ceram. Soc.*, 81 (1998) 106
30. M.C. Kuo and S.K. Yen, *Mater. Sci. Eng. C*, 20 (2002) 153
31. International Centre for Diffraction Data, Joint Committee on Powder Diffraction Standards, Powder Diffraction File, 1601 Park Lane, Swarthmore, PA 19081, USA (1988)
32. M.F. Hsieh, L.H. Perng, T.S. Chin and H.G. Perng, *Biomaterials*, 22 (2001) 2601
33. S.H. Kwon, Y. K. Jun, S. H. Hong and H.E. Kim, *J. Eur. Ceram. Soc.*, 23 (2003) 1039
34. M. Wei, A.J. Ruys, B.K. Milthorpe, C.C. Sorrell and J.H. Evans, *J. Sol–gel Sci. Technol.*, 21 (2001) 39
35. Z.-C. Wang, Y.-J. Ni and J.-C. Huang, *Biomed. Sci. Eng.*, 1 (2008) 190
36. M. Wei, A.J. Ruys, M.V. Swain, S.H. Kim, B.K. Milthorpe and C.C. Sorrell, *J. Mater. Sci.:Mater. Med.*, 10 (1999) 401
37. L. Müller and F. A. Müller, *Acta Biomater.*, 2 (2006) 181
38. S. Koutsopoulos, *J. Biomed. Mater. Res.*, 62 (2002) 600
39. D.A. Skoog, F.J. Holler and T.A. Nieman, *Principles in instrumental analysis*, 5th ed., Saunders Golden Sunburst Series, Philadelphia (1997)
40. M. V. Popa, J.M. C. Moreno, M. Popa, E. Vasilescu, P. Drob, C. Vasilescu and S.I. Drob, *Surf. Coating Techn.*, 205 (2011) 4776
41. S. Raynaud, E. Champion, D. Bernache-Assollant and P. Thomas, *Biomaterials*, 23 (2002) 1065
42. M.E. Orazem, B. Tribollet, *Electrochemical impedance spectroscopy*, A John Wiley & Sons, Inc, Hoboken, New Jersey (2008)
43. M.E. Orazem, N. Pebere and B. Tribollet, *J. Electrochem. Soc.*, 153 (2006) B129